Journal of Materials Research and Technology 39 (2025) 8994–9002

Contents lists available at ScienceDirect

Journal of Materials Research and Technology

journal homepage: www.elsevier.com/locate/jmrt

Nearly room-temperature fabrication of waste glass-derived foams for sustainable insulation

Muhammad J. Zafar, Lorenzo Moro, Hamada Elsayed, Enrico Bernardo *

Department of Industrial Engineering, Università Degli Studi di Padova, Padova, Italy

ARTICLE INFO

Keywords:
Glass waste
Weak alkaline suspensions
Glass foams
Thermal conductivity

ABSTRACT

A substantial proportion of glass waste is disposed of in landfills due to the limitations of conventional recycling methods in processing articles with specific chemical compositions or contamination, such as serigraphed glass, borosilicate glass, and glass mud residues. This study proposes an approach for managing such waste through the fabrication of highly porous, chemically stable glass foams at nearly room temperature, without the use of precious additives. Fine glass powders were homogeneously dispersed in weak alkaline suspensions, which were subsequently foamed by a combination of a limited amount of surfactant, foaming agent, and intensive mechanical stirring. The cellular structures were first stabilized through gelation and subsequently dried at 40 °C for 7 days. As an alternative, viscous flow sintering at 700 °C for 60 min was investigated as an end-of-life option for the first-generation green foams, resulting in porous glass-ceramic foams exhibiting an excellent strength-to-density ratio. The newly synthesized foams demonstrated an excellent compressive strength, ranging from 2 to 7 MPa, and a thermal conductivity of 0.13 W/m·°C, despite their high overall porosity of 68–73 %, which compares favourably to existing cement-based materials in terms of strength-to-density ratio and effective thermal conductivity.

1. Introduction

The rapid rise in population, urban development, and industrial activities has led to excessive waste generation and a growing need for housing [1]. This surge has significantly increased energy usage, along with higher greenhouse gas emissions [2]. By 2040, worldwide energy demand is projected to rise by 30 % [3]. Buildings alone account for nearly 40 % of global energy consumption [4], with a substantial portion used for heating and cooling to maintain indoor comfort, largely due to heat transfer through walls [5]. The European standard EN16798–3:2017 specifies that the optimal thermal transmittance (U-value) for building envelopes should be between 0.168 and 0.312 $W/m^2 \cdot K$ [6]. A lower U-value indicates better thermal efficiency [7]. Hence, incorporating high-performance insulation materials and effective design is crucial for energy-efficient construction [8]. This strategy appears promising in drastically cutting energy use, aligning with the goal of nearly zero-energy buildings [9]. Among insulating construction materials, glass-ceramic foams stand out as a reliable and sustainable option [10].

Aluminosilicate and glass-based foams are common examples of insulation materials made from waste. Unlike traditional options such as mineral wool and organic substances, which face challenges like flammability and recycling limitations, these foams are eco-friendly and fire-resistant [11,12]. They are produced by mixing crushed glass (cullet) with foaming agents and heating them beyond their softening point. This process releases gases, causing the glass to expand and form a porous structure with both open and closed cells [13]. Research on glass foam dates back to the 1930s, when it was first created using pure glass and the direct sintering method. Although initially expensive, the use of recycled glass and other inorganic waste, along with advancements in production techniques, eventually lowered costs and spurred industrial adoption [14]. Commercial glass foam typically has a compressive strength of 0.4–6.0 MPa, porosity ranging from 45 % to 85 % by volume, a bulk density of 0.1–1.2 g/cm^3, and thermal conductivity between 0.1 and 0.2 W/m·°C [15]. Thanks to these properties, it has become a preferred material for thermal and acoustic insulation in buildings [16].

Primary glass is commonly used in foam production, but the process is energy-intensive, particularly when using powdered glass or freshly obtained cullet. This method demands a two-stage heating process: first, melting raw glass at 1450–1500 °C, followed by sintering at 800–900 °C

* Corresponding author.
E-mail address: enrico.bernardo@unipd.it (E. Bernardo).

https://doi.org/10.1016/j.jmrt.2025.11.178
Received 25 August 2025; Received in revised form 14 October 2025; Accepted 21 November 2025
Available online 22 November 2025

[17]. Due to the high energy costs, researchers have long explored cheaper alternatives for producing glass-ceramic foams. One promising solution involves utilizing unrecycled waste glass to reduce expenses and energy consumption [18,19].

If discarded glass is not recycled into its original form (such as melting crushed containers to make new ones) in a closed-loop system, the alternative is open-loop recycling, where the glass is repurposed into entirely different products. This process can be referred to as upcycling if the new products generate profits higher than their production costs. Some waste glass has a negative value due to impurities or recycling challenges, making landfilling costly, prompting producers to seek alternative recycling methods. Utilizing low-energy processes, such as alkali activation at near-room temperature, can reduce processing costs. For example, turning cullet into glass foams offers an eco-friendly substitute for conventional foam glass production [20,21].

A recent study [22] has explored repurposing contaminated glass, such as pharmaceutical borosilicate glass, which cannot be conventionally remelted. A sustainable approach uses mild alkaline activation, where hydroxyl ions (OH^-) break surface Si–O–Si, Si–O–Al, and Si–O–B bonds, forming reactive Si–OH, Al–OH, and B–OH groups. Unlike the geopolymerization mechanism, this process mainly involves surface hydration of glass particles. The hardening mechanism occurs upon drying, where these surface hydroxyl groups on adjacent particles undergo a condensation reaction. This reforms strong chemical bridges (new Si–*O*–Si, Si–*O*–Al, and Si–*O*–B bonds) that bind the particles together. 'Welded' glass particles may trap hydrated alkali carbonates, resulting from the reaction between alkali cations and atmospheric CO_2, and a residual gel phase formed from the interaction of alkali with partially solubilized glass components.

The results reported by Taveri et al. [23], which describe the development of a stable gel network with a significant enrichment of BO_4 units, are valid only under specific activation conditions for example, when the glass is treated with a highly concentrated alkaline solution (13 M NaOH) together with additives rich in Al_2O_3, such as fly ash. In such cases, the dissolution and rearrangement of glass components in the alkaline medium leads to substantial gel formation. In the presence of substantial amounts of Al_2O_3 and B_2O_3 the gel exhibits an interconnected, three-dimensional zeolite-like network structure. In contrast, the gel phase from glass, activated without additives, by low molarity solutions (3 M NaOH, 'mild alkali activation') [22], is soluble (it may be removed by immersion of samples in boiling water). The key point, however, is the formation of a stable 'skeleton' of glass particles bridged by new Si–*O*–Si, Si–*O*–Al, and Si–*O*–B bonds.

The current study examines mild alkali activation of three distinct types of unrecycled glass waste by processing them into finely ground powders and treating them with a moderately dilute alkaline solution (3 M NaOH), followed by drying at 40 °C for seven days. The research proposes a distinct molecular mechanism for glass hardening, which is different from conventional geopolymerization processes. The resulting stable matrices, fabricated via direct foaming, demonstrate potential for the development of lightweight structural and insulating materials.

2. Materials and methods

Alkali-activated glass foams were produced using waste glass provided by Borgna Vetri Group in Cuneo, Italy. The waste consisted of coated (or 'serigraphed') glass (CG), i.e. fragments of enamelled glass sheets (manufactured by means of serigraphy), glass 'mud' from the cutting and drilling of coated and clean glass sheets (M), and borosilicate glass (BSG) The oxide-based chemical composition of the raw materials, determined through EDX analysis, is presented in Table 1.

The glass powders were produced through dry ball milling and then sieved to achieve particles smaller than 75 μm. Initially, the glass mud was dried at 75 °C for 12 h before being ball-milled into a fine powder. Sodium hydroxide (NaOH), a reagent-grade chemical from Sigma-Aldrich (Gillingham, UK), was used to create the alkaline solution.

Table 1
Chemical composition (wt.%) of raw materials.

Oxide (wt%)	CG	BSG	Glass Mud (M)
SiO_2	71.01	80.6	72.7
Na_2O	13.64	3.7	13.0
B_2O_3	–	12.2	–
CaO	10.60	–	9.1
MgO	3.53	–	3.5
Al_2O_3	0.49	2.6	0.9
Fe_2O_3	0.24	–	–
K_2O	0.12	0.9	0.2
SO_3	0.37	–	0.5

CG (Coated Glass), BSG (Borosilicate Glass).

The glass slurries were formed by soaking the glass powder in a 3 M NaOH solution, maintaining a liquid-to-solid weight ratio of 0.42. 3 M NaOH was selected as the optimal solution because it effectively activates different types of glass waste, enabling cold consolidation while maintaining environmental sustainability.

In the direct foaming process, the mixture was blended for 3 h at 500 rpm to obtain homogenous dissolution of glass particles at room temperature, before the addition of sodium perborate monohydrate ($NaBO_3{\cdot}H_2O$, Sigma Aldrich, Gillingham, UK) and sodium dodecyl sulphate (SDS, $CH_3(CH_2)_{11}OSO_3Na$, Sigma Aldrich, Gillingham, UK). Both additives were introduced at a concentration of 1 wt% relative to the solid content. Then, at the end mixture was stirred vigorously at 1200 rpm for 5 min. Vigorous mechanical stirring is used to force air into the liquid, creating bubbles. Then, the slurries were poured into open polystyrene molds (10 mm × 10 mm × 10 mm). The solid samples were then demolded following a 7-day drying period at 40 °C.

The cold-consolidated samples were subjected to comprehensive analysis, including destructive testing, starting with cubic blocks measuring approximately 10 × 10 × 10 mm^3. Select blocks from each formulation were preserved for further processing. The samples underwent heat treatment in a muffle furnace at 700 °C for 1 h, with a controlled heating rate of 1 °C/min. To replicate industrial conditions, cooling was accelerated by switching off the furnace and partially opening its door after the holding period, allowing natural cooling to room temperature. Table 2 outlines the sample labeling according to experimental parameters.

Geometric density (ρgeom) was calculated as the mass-to-volume ratio for uniform samples. Apparent density (ρapp) and true density (ρtrue) were measured using helium pycnometry (Ultrapyc 3000, Anton Paar GmbH, Graz, Austria) for both bulk and ground samples. From these measurements, open porosity (OP) and closed porosity (CP) were determined.

The compressive strength of the specimens (10 mm × 10 mm × 10

Table 2
Properties of samples made from activated waste glass powders and glass mud.

Sample type	ρgeom (g/cm3)	Total porosity (vol %)	Open porosity (vol %)	σc (MPa)	λ (W/(m•°C))
Coated Glass (CG)					
Unfired	0.74 ± 0.02	70 ± 3	66 ± 2	2 ± 0.5	0.19
Fired (700 °C)	0.68 ±.01	72 ± 4	68.5 ± 3	6.5 ±1	–
Mud 50 %+BSG 50 %					
Unfired	0.72 ± 0.02	69 ± 4	64 ± 2	2 ± 0.5	0.13
Fired (700 °C)	0.66 ± 0.02	71 ± 2	65 ± 1	5 ±0.5	–
BSG Foams					
Unfired	0.73 ± 0.02	67 ± 3	66 ± 1	7 ± 1.5	0.23
Fired (700 °C)	0.62 ± 0.01	72 ± 2	71 ± 2	7 ± 1	–

mm) was measured using a universal material testing machine (Quasar 25, Galdabini, Cardano, Italy) at a crosshead speed of 1 mm/min. For statistical reliability, a minimum of five specimens per sample were tested. Strength-density graphs were generated using data from both commercial building materials and experimental measurements. These analyses were performed with the CES (Cambridge Engineering Selector) software, part of Ansys Granta EduPack (Canonsburg, PA, USA).

The raw materials and reaction products were characterized using Fourier-transform infrared spectroscopy (FTIR) and X-ray diffraction (XRD). FTIR spectra were recorded on a Jasco 4200 spectrometer (Jasco, Japan) in absorbance mode, scanning the wavenumber range of 4000–400 cm^{-1} with 64 scans per sample to enhance signal-to-noise ratio. XRD analysis was performed using a Bruker D8 Advance diffractometer (Bruker AXS, Germany) equipped with CuKα radiation (40 kV, 40 mA). Data were collected over a 2θ range of 10°–70° at a step size of 0.02°. Phase identification was conducted semi-automatically via Match! ® software (Crystal Impact GbR, Germany), cross-referenced with the PDF-2 database (ICDD, USA).

The microstructures were examined using optical microscopy (OM) with an AxioCam ERc 5s microscope camera (Carl Zeiss Microscopy, Thornwood, NY, USA) as well as scanning electron microscopy coupled with energy-dispersive X-ray spectroscopy (SEM-EDS, FEI Quanta 200 ESEM, Eindhoven, Netherlands).

To evaluate stability, the samples were immersed in boiling water for 3 h, and their mass changes were measured after a 7-day drying period.

A thermal conductivity test was carried out on specific 'as-cast' samples (40 mm × 40 mm × 10 mm) using the Transient Plane Source (TPS) method. The setup involved placing two samples on either side of a sensor (Hot Disk AB, Göteborg, Sweden, model 8563, with a radius of 9.863 mm), which contained a double-spiral nickel resistance element encased in Kapton layers. The sensor, heated by a constant electric current, recorded temperature changes to determine thermal conductivity. For the chosen foam formulation, five measurements were taken at room temperature (22 ± 2 °C), with a fixed power of 100 mW and a measurement duration of 160 s.

3. Results and discussion

3.1. Alkali activation and foaming of glass powders

Three different types of glass waste were selected for this study due to their challenging recyclability and unique chemical compositions. Previous research on mild alkali activation [24] suggests that the hardening of activated suspensions does not result from the formation of a specific binding phase. Instead, the gel-forming compounds produced by the same activator (NaOH) vary depending on the glass chemistry. When using low-concentration alkali solutions, only minimal glass dissolution occurs. The hardening mechanism likely involves condensation reactions between hydrated layers on particle surfaces, resulting in the formation of Si–O–Si bonds. Dissolved silicates, borates, and aluminates combine with alkaline ions, generating soluble secondary phases. Although some components may contribute to gel formation, this gel has a negligible effect on the material's overall strength development [25,26].

Fig. 1 displays the diffraction patterns of the foams in their as-received state, after hardening, boiling, and firing at 700 °C. The XRD patterns in Fig. 1a and b show no significant contamination from crystalline phases, instead exhibiting a broad asymmetric hump with peaks at approximately 2θ~23–24° and 2θ~21–22°, respectively. However, in the case of the BSG + Mud raw mixture (Fig. 1c), calcite ($CaCO_3$, PDF #00-002-0623) peaks appear above the background. This contamination likely results from reactions that occur in the mud during transport, before it is dried.

The hardening of alkali-activated slurries occurs when glass powder partially dissolves, followed by condensation reactions that create strong bonds between particles. Dissolved glass components reorganize into carbonates (due to atmospheric interaction) and an amorphous gel phase (facilitated by alkaline ions). A noticeable shift in the amorphous background confirms the formation of an additional gel phase. In the XRD patterns (Fig. 1a for coated glass and Fig. 1b for borosilicate glass), the sole crystalline phase identified is sodium hydrogen carbonate hydrate (PDF#00-029-1447). However, the diffraction pattern for BSG + Mud (Fig. 1c) shows new phases, including sodium carbonate hydrate

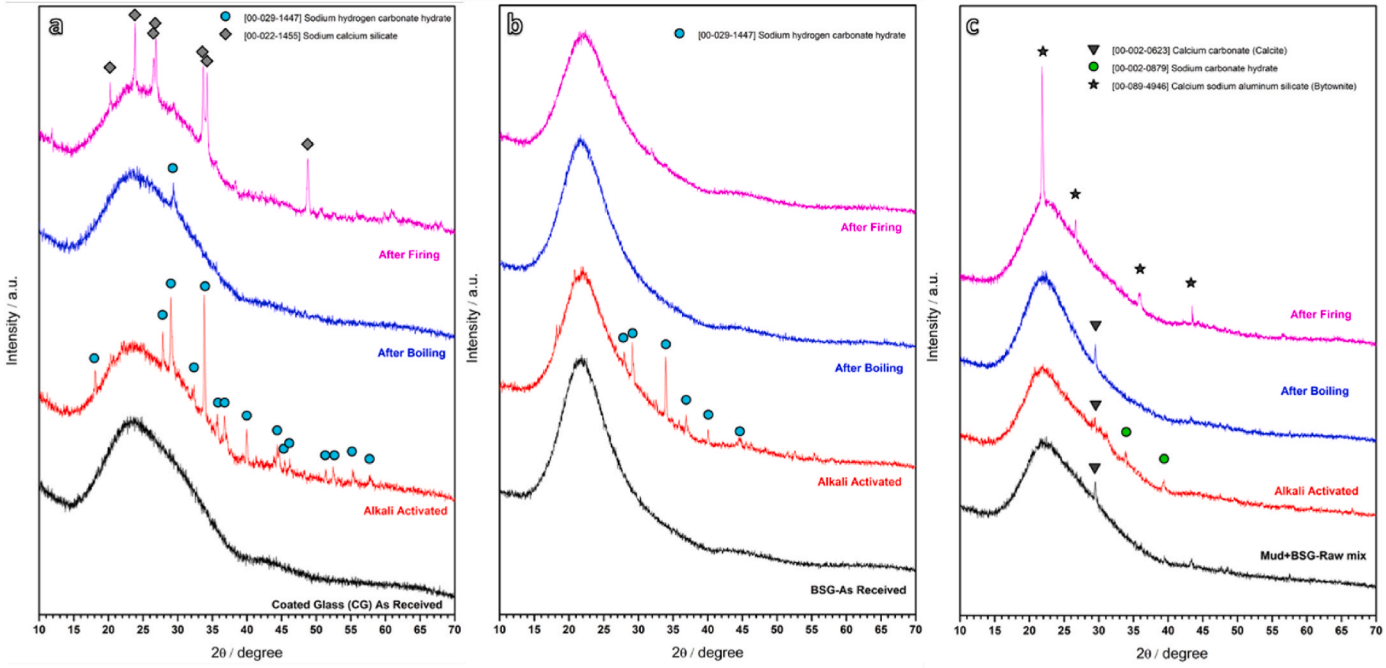

Fig. 1. – X-ray diffraction analysis of glass powders and BSG + Mud composites in the received state, after activation, after boiling, and firing; a) Coated glass, b) Borosilicate glass (BSG), c) BSG + Mud composite.

(PDF#00-002-0879) alongside pre-existing calcium carbonate ($CaCO_3$, PDF#00-002-0623) [27]. Notably, the gel produced after alkali activation initially obscured the intensity of crystalline phases, which became more distinct after boiling.

Typically, carbonates dissolve in water [28], which is why, apart from a small peak in coated glass, they are no longer detectable in boiled samples, as seen in Fig. 1a and b. While calcium carbonate ($CaCO_3$, PDF#00-002-0623) has limited solubility in water, traces of it from the initial raw mixture remain observable in the boiled composites.

When coated glass samples were heated to 700 °C, a notable formation of sodium calcium silicate (PDF#00-022-1455) occurred (Fig. 1a). This crystalline phase is commonly produced during the devitrification of soda-lime glass, likely facilitated by the breakdown of gels into an alkali-rich glass [29]. In contrast, borosilicate glass (BSG) retains its amorphous structure after the same heat treatment. However, the broad "halo" in their diffraction patterns shifted slightly to lower angles (Fig. 1b). This shift suggests the breakdown of hydrated compounds and the integration of oxides into new glass matrices, leaving only the effects of alkali incorporation. However, after firing at 700 °C, the BSG + Mud composite exhibits an intense peak corresponding to Calcium sodium aluminum silicate-Bytownite (PDF#89–4946) (Fig. 1c).

Infrared spectroscopy (Fig. 2) provides insights into the compounds formed during drying and their transformations upon firing. In Fig. 2a (coated glass), the peak near 1445 cm^{-1} aligns with observations for C–S–H gels, suggesting the presence of carbonate compounds under activated conditions, which vanish after boiling. Notably, the band around 960 cm^{-1}, linked to the asymmetric stretching of Si–*O*–Si and Si–*O*–Al bonds, is crucial for binding glass particles [30]. The shift of this band to higher wavenumbers with alkali activation indicates the breakdown of Si–*O*–Si and Al–*O*–Si bonds, leading to an increase in non-bridging oxygen atoms.

Fig. 2 (b and c) presents the findings of Fourier Transform Infrared (FT-IR) spectroscopy, offering additional evidence regarding the response of borosilicate glass and the BSG + Mud composite to alkali activation. The initial material displays characteristic absorption bands associated with asymmetric stretching vibrations of Si–*O*–Si and Si–*O*–Al linkages (centred around 1040 cm-1 and 1013 cm^{-1}, respectively), [BO_4] vibrations, Si–*O*–B stretching vibrations (manifested as a broad signal at 910 cm^{-1}, symmetric stretching vibrations of Si–*O*–Si, and [BO_3] vibrations (indicated by a peak at 665 cm-1. Furthermore, the band at 785 cm-1 is attributed to the symmetric stretching vibration of O–Si–O units. The alkali activation process is suggested by a bathochromic shift of the principal absorption peak, indicative of mixed-ion gel formation (995-985 cm^{-1}), alongside the emergence of a new signal within the (1460−1432 cm^{-1} range), corresponding to the formation of carbonate species [30].

Interestingly, the FT-IR spectrum of the material after boiling remains practically identical to that of the starting material, as shown in Fig. 2. This suggests that the spectral changes observed upon activation arise from the overlapping signals of the largely unmodified glass matrix and additional phases, such as alkali carbonates and gel. These secondary phases likely form from components released into the solution due to the partial disruption of the glass network (e.g., silicate, borate, and aluminate ions) [22]. The gel's high alkali content likely results in low network connectivity, characterized by a limited number of bridging oxygens, which leads to poor chemical stability.

3.2. Morphology and mechanical properties of cold-consolidated and fired bodies

Fig. 3 presents the scanning electron microscopy (SEM) images illustrating the microstructure of cold-consolidated "green" foams produced from different waste glass precursors. The foams exhibit a homogeneous, open-celled, and crack-free morphology, which was successfully achieved through oxygen release (from perborate turning into borate) during drying and consolidation. This simple and energy-efficient process ensured uniform dispersion of the activating agents and effective pore formation throughout the matrix.

As shown in Fig. 3a, b and summarized in Table 2, the coated glass waste was transformed into a *hierarchical* porous structure with a total porosity of approximately 70 vol%, predominantly consisting of interconnected open pores. Higher-magnification SEM images further revealed that the cell walls were relatively thin and not fully compact, suggesting that pore development was governed by gas release and particle rearrangement during the consolidation process.

The alkali-activated green glass foam exhibited a bulk density of 0.74 g/cm^3 and a total porosity of 70 %. Despite its lightweight nature, the foam demonstrated a compressive strength of 2 MPa, which surpasses that of conventional lightweight insulating concretes of similar strength levels while maintaining a significantly lower density, as illustrated in Fig. 4. This combination of low density and adequate strength highlights the material's potential for use in structural insulation and sustainable construction applications.

Furthermore, the coated glass-derived green foam compares favourably with commercial glass foams in terms of compressive strength. Although its density is slightly higher than that of typical commercial foams, the mechanical performance and eco-friendly production route make it a promising candidate for substituting conventional materials in lightweight building systems and thermal insulation panels.

As illustrated in Fig. 3(c) and (d), the alkali-activated composite (BSG + Mud) green glass foam exhibits a highly porous architecture, primarily consisting of open pores evenly dispersed throughout the matrix. The pore structure varies notably between the composite and other samples due to differences in the initial slurry viscosity. The addition of ultra-fine glass mud powder slightly increases viscosity,

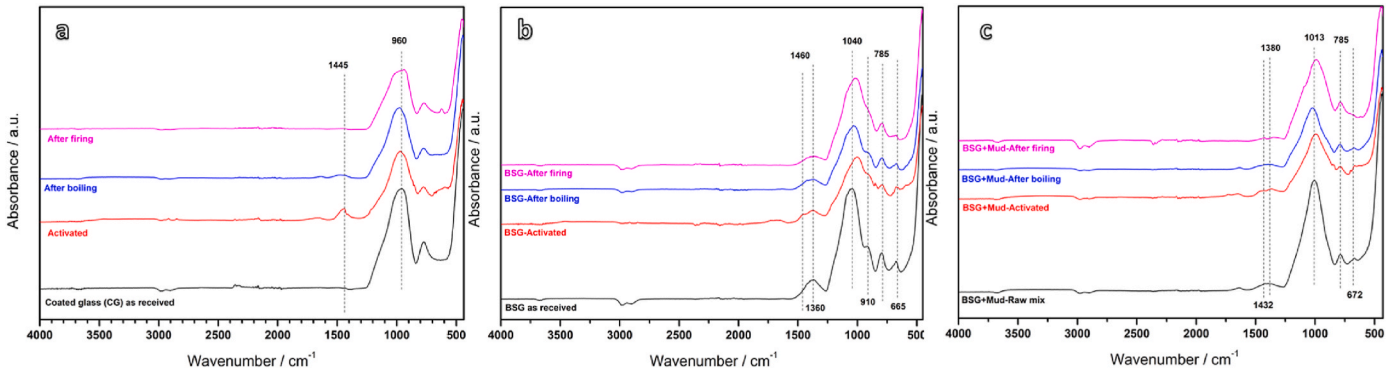

Fig. 2. FTIR analysis of glass powders and BSG + Mud composites in the received state, after activation, after boiling, and firing; a) Coated glass, b) Borosilicate glass (BSG), c) BSG + Mud composite.

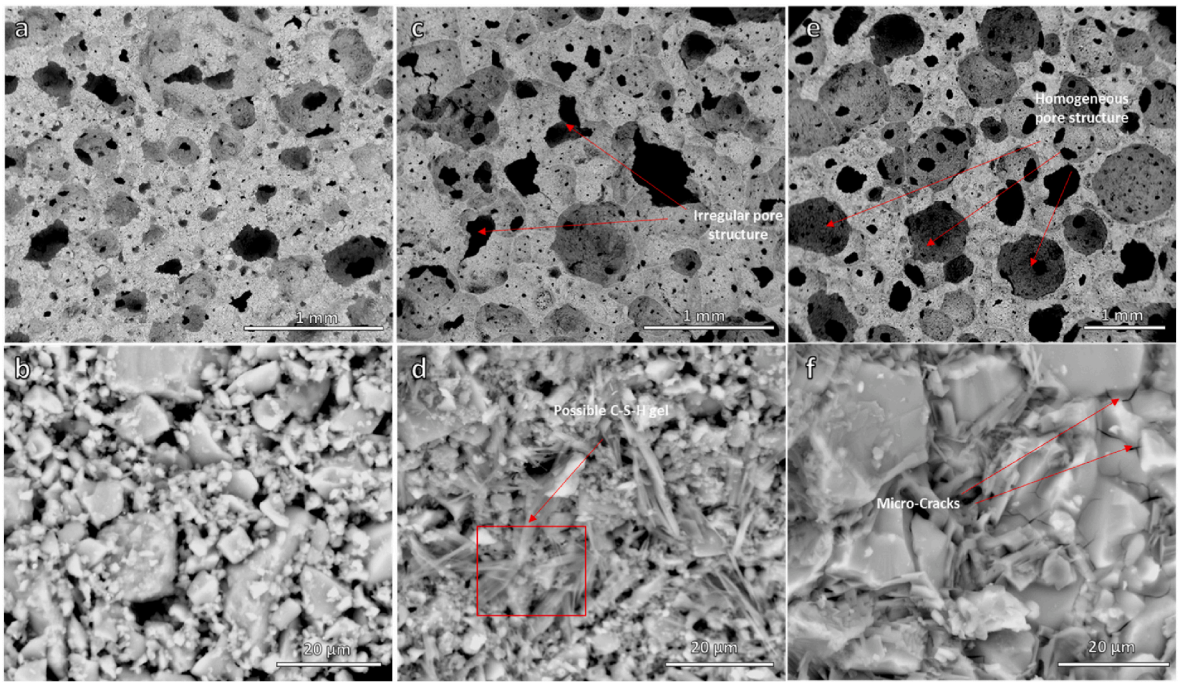

Fig. 3. Microstructural details of activated green samples: a,b) coated glass; c,d) BSG + Mud composite; e,f) borosilicate glass.

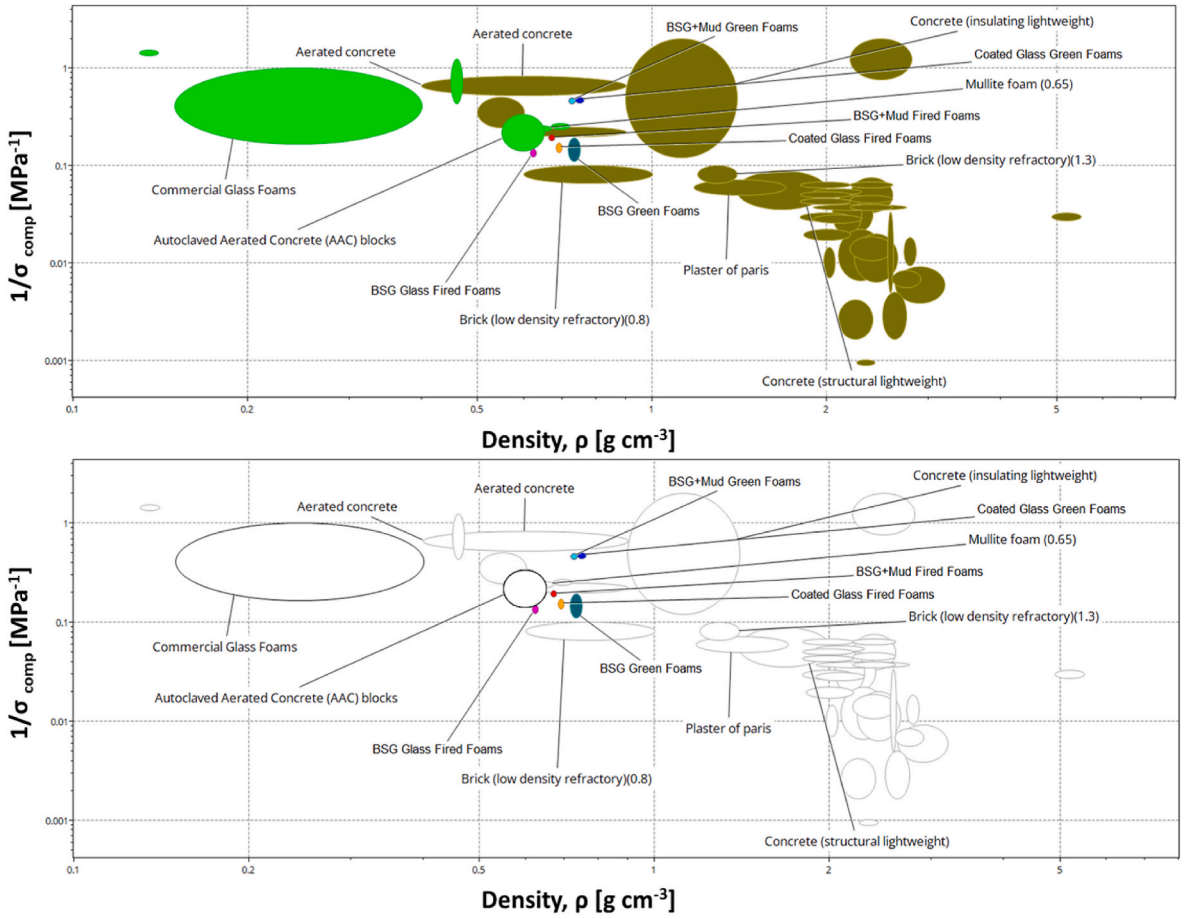

Fig. 4. Strength/density trade-offs, for comparing developed materials with already available commercial materials, compressive strength (computed using CES software package) – the graph reported below is intended to highlight the positions of experimental samples.

causing the pores to shift from a spherical shape to an irregular, polygonal form. SEM imaging shows a partially reacted glassy phase within a dense C–S–H gel matrix, with no visible microcracks typically associated with drying shrinkage. The foam has a low bulk density (0.72 g/cm^3) and high porosity (~70 %), along with a compressive strength of 2 MPa, making it ideal for thermal insulation. According to Fig. 4 and Table 2, the composite green foam's mechanical and physical properties closely resemble those of coated glass green foams, positioning it as an excellent alternative to lightweight insulating concrete.

As illustrated in Fig. 3(e) and (f), borosilicate green glass foam exhibits a highly porous, interconnected structure with pores varying in size from macropores (>50 μm) to micropores (<10 μm). Most pores are spherical, although some appear elongated or collapsed, likely due to the release of gas during the foaming process. The pore walls are dense and glassy, with occasional microcracks formed from shrinkage during drying (Fig. 3f). Additionally, remnants of borosilicate glass can be seen as angular or partially dissolved particles within the matrix. With a density of 0.73 g/cm^3 and a compressive strength of 7 MPa, borosilicate green glass foam demonstrates mechanical performance comparable to that of low-density construction materials such as lightweight bricks, mullite foams, and Autoclaved Aerated Concrete (AAC) blocks.

Notably, they exceed the compressive strength of conventional commercial glass at slightly higher density. This places them in a unique category as a "non-dominated" material, meaning that no other commercially available material offers a higher compressive strength at the same density level. Consequently, these glass foams represent an optimal balance between lightness and mechanical performance, making them highly attractive for applications requiring both structural integrity and weight reduction. Among the three types of glass foams, borosilicate glass foams exhibit superior compressive strength, primarily due to their unique chemical composition and structural stability. Additionally, borosilicate glass foams often exhibit a more uniform pore distribution and stronger cell walls due to their more uniform and interconnected pore structure, as observed in the microstructural analysis (Fig. 3e and (f)), which effectively distributes stress and reduces localized failure points. These combined factors give borosilicate glass foams superior mechanical integrity, durability, and stability under both thermal and mechanical loads.

The lower compressive strength of the alkali-activated (BSG + Mud) composite compared to pure borosilicate glass is mainly due to changes in pore morphology. The addition of ultra-fine glass mud increases the slurry viscosity, leading to the formation of irregular, polygonal pores rather than uniform spherical ones. These irregular pores act as stress concentrators, weakening the matrix and reducing its compressive capacity despite partial densification from the mud.

Cold-consolidated foams, produced through mild alkali activation followed by simple drying of glass foam suspensions, can be regarded as first-generation products. The application of heat treatment, as a secondary processing step, offers a pathway to recycle these first-generation materials at the end of their life cycle. This approach enables their use as effective precursors for the production of porous glass-ceramics, resulting in second-generation products.

Heating at 700 °C with a slow ramp rate of 1 °C/min (intended to remove the surfactant) resulted in notable changes to the cellular structure, particularly for coated glass foams. The resulting foams exhibited greater uniformity after firing. As indicated in Table 2, the total porosity rose following the 700 °C treatment, demonstrating that glass foaming is not a static process limited to bubble nucleation and growth within the softened, pyroplastic glass. Instead, bubbles can collapse and be succeeded by newly formed ones [29], as illustrated in Fig. 5(a and b).

The coated glass foams demonstrated a crushing strength exceeding 6 MPa and a density of 0.68 g/cm^3, with a total porosity of over 72 %. As illustrated in Fig. 5 and Table 2, these properties make them an excellent substitute for low-density bricks and mullite foams.

After being fired at 700 °C, both composite foams and borosilicate foams stayed mostly amorphous, as shown by the X-ray diffraction pattern in Fig. 1. However, noticeable changes occurred due to viscous flow remodelling, leading to significant cell coarsening (Fig. 5d and f). The high open porosity observed might not reflect an interconnected pore network but could instead result from gas trapped in large surface bubbles on the samples.

The firing process not only caused dehydration but also led to the gel being absorbed into the molecular structure of BSG (borosilicate glass). This resulted in the incorporation of additional Na^+ ions from the activating solutions, forming extra BO_4 and AlO_4 units within the glass

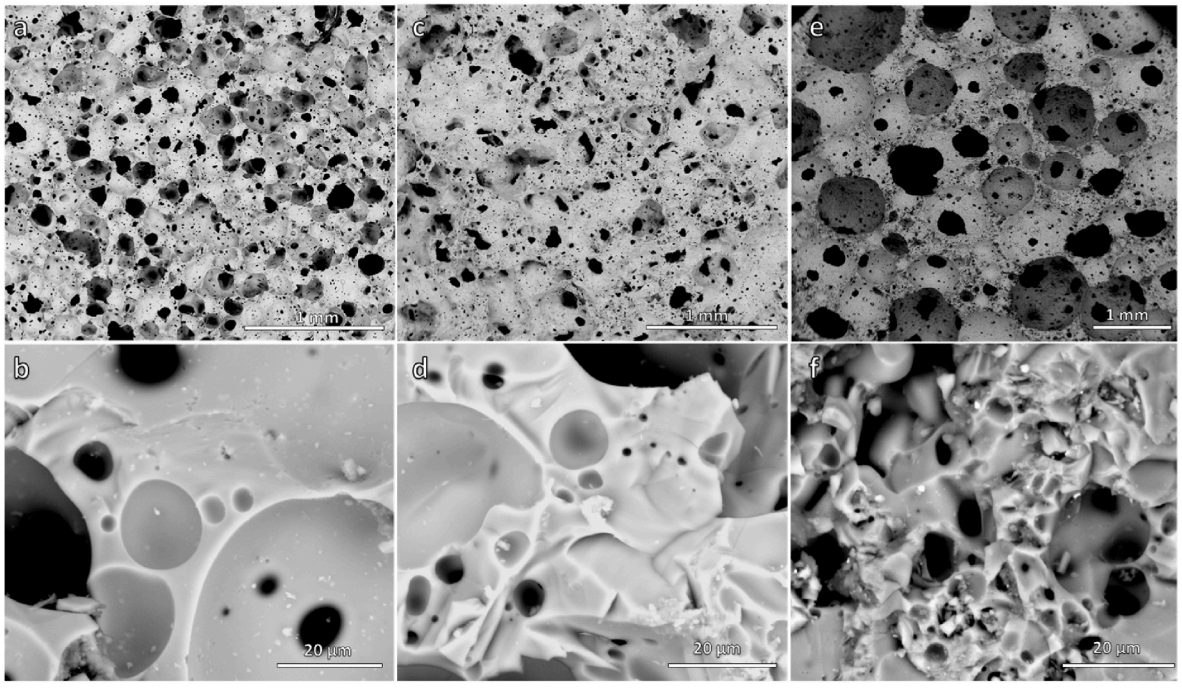

Fig. 5. Microstructural details of samples after firing at 700 °C: a,b) coated glass; c,d) BSG + Mud composite; e,f) borosilicate glass.

structure. The open-cell morphology observed in the 'green' state was preserved after firing for both activating solutions, as seen in Fig. 5. The firing temperature used was apparently insufficient to significantly soften the BSG. Additionally, the low amount of hydrated phase prevented secondary foaming and pore reshaping, a phenomenon observed in coated soda-lime glass [29,31]. Instead, water vapor release likely caused only small micropores, visible as darker spots on the struts (Fig. 5d and f).

As indicated in Table 2 and Fig. 5(c) and (d), the fired composite foams exhibited a notable compressive strength of 5.5 MPa, with a density of 0.66 g/cm^3, resulting in an overall porosity of 72 %. This makes them a strong alternative to mullite foams and low-density bricks, due to their significantly lower densities. Meanwhile, borosilicate glass foams maintained their compressive strength at 7 MPa after firing, despite a slight reduction in density (0.62 g/cm^3).

Firing at 700 °C provides an optimal compromise between energy efficiency, material performance, and process sustainability. Operating at this relatively lower temperature significantly reduces the overall energy consumption of the thermal treatment stage, as less heat input is required to reach and maintain the target temperature. The shorter dwell times associated with firing at 700 °C further enhance production efficiency by minimizing the duration of exposure in the furnace, which in turn lowers fuel usage, operational costs, and the carbon footprint of the manufacturing process.

From a materials science perspective, firing at this temperature is sufficient to promote the viscous flow sintering and pore formation necessary for producing a stable and homogeneously structured glass foam, while avoiding the detrimental effects associated with higher firing regimes. When firing temperatures exceed approximately 800–900 °C, there is an increased tendency for crystallization or devitrification within the glass matrix. Such structural changes can lead to a loss of porosity, reduced mechanical integrity, and compromised thermal insulation performance, all of which are undesirable for the intended applications.

By maintaining the firing temperature at 700 °C, the process achieves a favorable balance, preserving the desired cellular morphology, maintaining thermal stability, and ensuring that the resulting material meets the performance requirements for lightweight, insulating glass foams. Overall, our findings indicate that 700 °C represents a sustainable, cost-effective, and technically sound firing condition that aligns with both industrial efficiency goals and environmental responsibility, without sacrificing material quality or functional performance.

Fig. 6 illustrates the thermal insulation potential of the developed green samples. All three types of green foams demonstrate excellent thermal insulation capabilities, with thermal conductivity values comparable to those of well-established mullite foams and Autoclaved Aerated Concrete (AAC) blocks. In addition to their favorable thermal performance, these foams exhibit mechanical properties similar to those of aerated concrete, while offering notably superior thermal efficiency, particularly through their significantly lower thermal conductivity.

Among the tested materials, the green glass foam composites (BSG + Mud) stand out as exceptional thermal insulators, achieving a remarkably low thermal conductivity of 0.13 W/m·°C. This value not only surpasses that of aerated concrete but also outperforms high-performance ceramic foams such as mullite foams, highlighting the strong potential of these composites for energy-efficient applications.

It is also observed that thermal conductivity tends to increase with larger pore sizes, indicating a direct relationship between the foam's microstructure and its insulating performance. Notably, borosilicate glass foams exhibit the highest thermal conductivity among the samples, with a measured value of 0.23 W/m·°C, indicating that pore morphology and composition play a critical role in determining the overall thermal behaviour of these materials.

3.3. Boiling test

The boiling water test in geopolymer studies evaluates the material resistance to high temperatures and its ability to maintain structural integrity when exposed to boiling water [32,33]. If the composition lacks the right balance of key components (such as alkali oxides, Al_2O_3, and SiO_2), condensation reactions may still cause gelation, but the resulting material remains unstable and dissolves in water. This behavior mirrors that of low-connectivity glasses, which contain high amounts of network modifiers and have fewer bridging oxygen bonds.

In the current study, all green specimens passed the boiling water test with no surface cracks or breaks, confirming the solid internal structure and indicating the material's ability to maintain its structure and properties when exposed to hot water, as shown in Table 3. There is a minor change in mass percentage (ΔM%) after boiling.

The samples subjected to cold consolidation exhibited structural integrity upon boiling in water, maintaining stability even after prolonged immersion periods of 180 min (Fig. 7). This observed durability indicates the formation of robust bridging bonds, strong chemical

Table 3
ΔM (%) after boiling of green foamed samples.

Sample type	Before boiling mass	After boiling mass	After boiling ΔM (%)
Coated glass (CG)	1.21	1.15	4.96 ± 1
Mud 50 %+BSG 50 %	0.83	0.80	3.61 ± 1
BSG Foams	0.59	0.57	3.39 ± 0.5

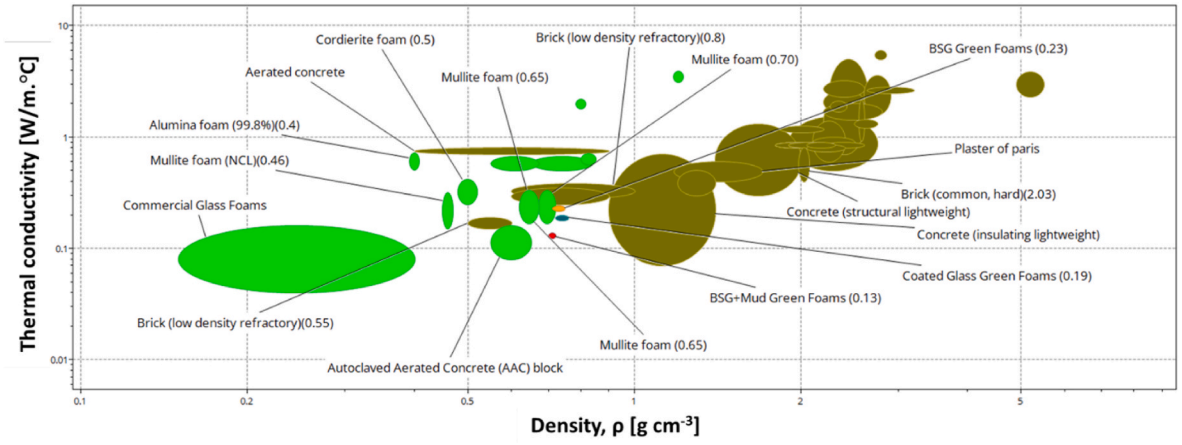

Fig. 6. Thermal Conductivity/density trade-offs, for comparing developed materials with already available commercial materials (computed using CES software package).

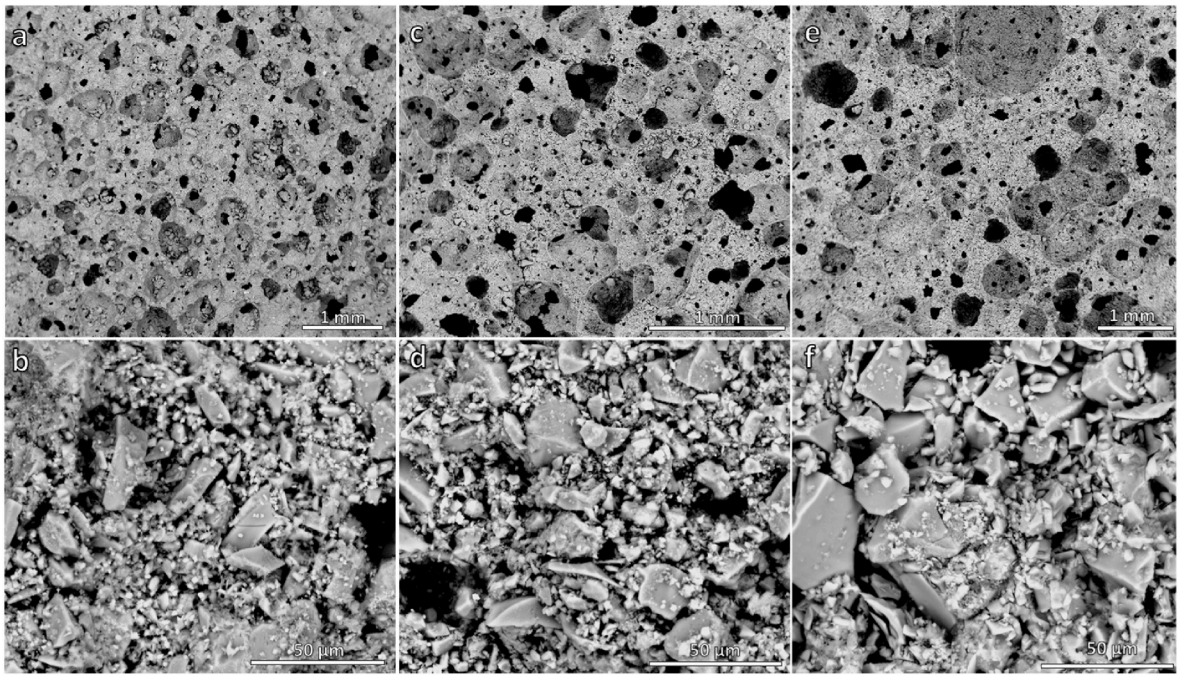

Fig. 7. Microstructural details of samples after boiling: a,b) coated glass; c,d) BSG + Mud composite; e,f) borosilicate glass.

linkages between the glass particles. These bonds may originate from distinct atomic-scale configurations, classified as either 'zeolite-like' or 'non-zeolitic'. In the zeolite-like configuration, adjacent glass particles are interconnected via a network of SiO_4, AlO_4, and BO_4 tetrahedral units, analogous to the structural frameworks found in geopolymers. Here, alkali cations stabilize the coordination geometry of Al and B. This bonding mechanism involves the precipitation of a highly crosslinked gel, formed from dissolved ionic species, which acts as a binding matrix between particles. Conversely, the non-zeolitic arrangement features simpler bridging structures, predominantly mediated by oxygen atoms. Upon exposure to OH^- ions (from the alkaline activator), hydrolysis of Si–*O*–Si, Si–*O*–Al, and Si–*O*–B bonds occurs, resulting in the formation of a hydrated interfacial layer enriched with Si–OH, Al–OH, and B–OH terminal groups. These reactive hydroxyl groups facilitate interparticle condensation, reforming the original covalent bonds and enabling effective particle welding [28].

Fig. 7 presents SEM images of the materials under investigation before and after the boiling test. The alkali-activated sample's structure indicates minimal dissolution of the raw materials, with many particles remaining unreacted. A thin film partially coats the glass particles, binding them together. Although boiling did not separate neighbouring particles, the gaps between them suggest the leaching of a soluble component.

4. Conclusion

Mild alkali activation offers a promising and feasible approach for the open-loop recycling of challenging glass waste, transforming it into highly porous, mechanically robust, and chemically stable glass foams through an energy-efficient process that involves room-temperature gelation and low-temperature sintering. This method leverages controlled chemical reactions between waste glass and alkaline solutions to form a stable gel network, which is then sintered at relatively low temperatures (typically below 800 °C) to produce a lightweight, cellular structure. The resulting foams exhibit an optimal balance of high porosity (68–73 %) and exceptional mechanical strength, with compressive strengths ranging from 2 to 7 MPa, comparable to or even surpassing some conventional cement-based materials. Additionally, these foams demonstrate excellent thermal insulation properties, with an effective thermal conductivity as low as 0.13 W/m·°C, making them competitive with commercially available insulating materials.

Beyond their performance metrics, this recycling strategy addresses critical environmental challenges by utilizing non-recyclable glass waste, often destined for landfills, into high-value construction applications. The process is not only sustainable (reducing raw material extraction and energy consumption compared to traditional foam production) but also scalable, as it utilizes widely available waste streams and simple processing steps. Potential applications include lightweight structural panels, insulation layers in buildings, and acoustic damping materials, all of which contribute to energy-efficient construction practices. By valorising otherwise discarded glass, this approach aligns with circular economy principles, offering a dual benefit of waste mitigation and resource-efficient material innovation.

CRediT authorship contribution statement

Muhammad J. Zafar: Writing – original draft, Investigation, Formal analysis, Data curation, Conceptualization. **Lorenzo Moro:** Investigation, Data curation. **Hamada Elsayed:** Investigation, Data curation. **Enrico Bernardo:** Writing – review & editing, Supervision, Visualization, Resources, Methodology, Funding acquisition, Conceptualization.

Declaration of competing interest

The authors declare that they have no known competing financial interests or personal relationships that could have appeared to influence the work reported in this paper.

Acknowledgements

M.J.Z. and E.B. acknowledge the support from the Italian Ministry of University & Research (MUR), through Next Generation EU funds, in the framework of the DM588 PhD Scholarship program in cooperation with Borgna Vetri S.r.l. (Cuneo, Italy); E.B. also acknowledges the Italian Ministry of University & Research (MUR), through Next Generation EU funds, in the framework of PRIN 2022 PNRR project GLASS_Trea.S.U.

Res (GLASS-based TREAtments for Sustainable Upcycling of inorganic RESidues, #P2022S4TK2).

Data availability

Data will be made available on request.

References

[1] Kravchenko E, Lazorenko G, Jiang X, Leng Z. Alkali-activated materials made of construction and demolition waste as precursors: a review. Sustain Mater Technol 2024;39:e00829.
[2] Zarco-Soto FJ, Zarco-Soto IM, Ali SSS, Zarco-Periñán PJ. Energy consumption in buildings: a compilation of current studies. Energy Rep 2025;13:1293–307.
[3] Ahmad T, Zhang D. A critical review of comparative global historical energy consumption and future demand: the story told so far. Energy Rep 2020;6:1973–91.
[4] Pais-Magalhães V, Moutinho V, Robaina M. Is an ageing population impacting energy use in the european union? Drivers, lifestyles, and consumption patterns of elderly households. Energy Res Social Sci 2022;85:102443.
[5] Yu J, Lu Y, Hu J, Zhong K, Jia T, Yang X. Prediction models for building thermal mass of intermittently heated rooms for balancing energy consumption and indoor thermal comfort. Energy Build 2024;317:114376.
[6] Ahmed K, Carlier M, Feldmann C, Kurnitski J. A new method for contrasting energy performance and near-zero energy building requirements in different climates and countries. Energies 2018;11:1334.
[7] Wang Z, Zhao J. Optimization of passive envelop energy efficient measures for office buildings in different climate regions of China based on modified sensitivity analysis. Sustainability 2018;10:907.
[8] Bibri SE, Huang J, Omar O, Kenawy I. Synergistic integration of digital twins and zero energy buildings for climate change mitigation in sustainable smart cities: a systematic review and novel framework. Energy Build 2025;333:115484.
[9] Shi X, Liao Q, Chen K, Wang Y, Liu L, Wang F, Zhu H, Zhang L, Liu C. Foaming process and thermal insulation properties of foamed glass-ceramics prepared by recycling muti-solid wastes. Constr Build Mater 2025;466:140270.
[10] Li T, He G, Jiang Z, Duan Y, Liu M. Research advances and new insights into multi-source solid waste-derived ceramic foams. Sustain Mater Technol 2025;45:e01535.
[11] Islam S, Bhat G. Environmentally-friendly thermal and acoustic insulation materials from recycled textiles. J Environ Manag 2019;251:109536.
[12] Urdanpilleta M, Leceta I, Martín-Garín A, Millán-García JA, Guerrero P, Caba Kdl. Valorized sheep wool biocomposites towards a more sustainable building sector: thermal insulation, sound absorption, and resistance against insects. Dev Built Environ 2025;21:100608.
[13] Liu T, Liu P, Guo X, Zhang J, Huang Q, Luo Z, Zhou X, Yang Q, Tang Y, Lu A. Preparation, characterization and discussion of glass ceramic foam material: analysis of glass phase, fractal dimension and self-foaming mechanism. Mater Chem Phys 2020;243:122614.
[14] Bernardo E, Cedro R, Florean M, Hreglich S. Reutilization and stabilization of wastes by the production of glass foams. Ceram Int 2007;33(6):963–8.
[15] Barbosa ARJ, Lopes AAS, Sequeira SIH, Oliveira JP, Davarpanah A, Mohseni F, Amaral VS, Monteiro RCC. Effect of processing conditions on the properties of recycled cathode ray tube glass foams. J Porous Mater 2016;23(6):1663–9.
[16] Benli A. Sustainable use of waste glass sand and waste glass powder in alkali-activated slag foam concretes: Physico-mechanical, thermal insulation and durability characteristics. Constr Build Mater 2024;438:137128.
[17] Kazantseva LK, Rashchenko SV. Optimization of porous heat-insulating ceramics manufacturing from zeolitic rocks. Ceram Int 2016;42(16):19250–6.
[18] Zafar MJ, Elsayed H, Bernardo E. Waste glass upcycling supported by alkali activation: an overview. Materials 2024;17:2169.
[19] Özkılıç YO, Çelik Aİ, Tunç U, Karalar M, Deifalla A, Alomayri T, Althoey F. The use of crushed recycled glass for alkali activated fly ash based geopolymer concrete and prediction of its capacity. J Mater Res Technol 2023;24:8267–81.
[20] Xiao R, Dai X, Zhong J, Ma Y, Jiang X, He J, Wang Y, Huang B. Toward waste glass upcycling: preparation and characterization of high-volume waste glass geopolymer composites. Sustain Mater Technol 2024;40:e00890.
[21] Cozzarini L, De Lorenzi L, Fortuna L, Bevilacqua P. Recycling of glass waste and spent alkaline batteries cathodes into insulation materials. Sustain Mater Technol 2023;38:e00767.
[22] Tameni G, Lago D, Kaňková H, Buňová L, Kraxner J, Galusek D, Dawson DM, Ashbrook SE, Bernardo E. Alkaline attack of boro-alumino-silicate glass: new insights of the molecular mechanism of cold consolidation and new applications. Open Ceramics 2025;21:100726.
[23] Taveri G, Tousek J, Bernardo E, Toniolo N, Boccaccini AR, Dlouhy I. Proving the role of boron in the structure of fly-ash/borosilicate glass based geopolymers. Mater Lett 2017;200:105–8.
[24] Lago D, Tameni G, Zorzi F, Kraxner J, Galusek D, Bernardo E. Novel cesium immobilization by alkali activation and cold consolidation of waste pharmaceutical glass. J Clean Prod 2024;461:142673.
[25] Carollo F, Rienzo ED, D'Angelo A, Sgarbossa P, Barbieri L, Leonelli C, Lancellotti I, Catauro M, Bernardo E. Cold consolidation of waste glass by alkali activation and curing by traditional and microwave heating. Materials 2025;18:2628.
[26] Rincón Romero A, Toniolo N, Boccaccini AR, Bernardo E. Glass-ceramic foams from 'Weak Alkali Activation' and gel-casting of waste Glass/Fly ash mixtures. Materials 2019.
[27] Lago D, Kraxner J, Galusek D, Bernardo E. Development of porous membranes by alkali activation of borosilicate glass: effect of wastewater acidity on copper adsorption. Dev Built Environ 2025;23:100705.
[28] Tameni G, Carollo F, Cavazzini AM, Forzan M, Bernardo E. Microwave assisted cold consolidation of alkali activated suspension of glass waste powders. Mater Lett 2025;389:138354.
[29] Rincón A, Giacomello G, Pasetto M, Bernardo E. Novel 'inorganic gel casting' process for the manufacturing of glass foams. J Eur Ceram Soc 2017;37(5):2227–34.
[30] Cammelli F, Tameni G, Bernardo E. Sustainable stabilization of waste foundry sands in alkali activated glass-based matrices. Case Stud Constr Mater 2024;21:e03538.
[31] Rincon Romero A, Tamburini S, Taveri G, Toušek J, Dlouhy I, Bernardo E. Extension of the 'Inorganic Gel Casting' process to the manufacturing of boro-alumino-silicate glass foams. Materials 2018;11:2545.
[32] Xiao R, Polaczyk P, Wang Y, Ma Y, Lu H, Huang B. Measuring moisture damage of hot-mix asphalt (HMA) by digital imaging-assisted modified boiling test (ASTM D3625): recent advancements and further investigation. Constr Build Mater 2022;350:128855.
[33] Catauro M, Viola V, D'Amore A. Mosses on geopolymers: preliminary durability study and chemical characterization of metakaolin-based geopolymers filled with wood ash. Polymers 2023;15:1639.